UNLIMITED

TR 90032

ROYAL AEROSPACE ESTABLISHMENT

Technical Report TR 90032

June 1990

The Stereoscopic Geometry of the Remote Sensing 'Optical Mapping Instrument'

by

N. S. Wells

Procurement Executive, Ministry of Defence
Farnborough, Hampshire

UNLIMITED

CONDITIONS OF RELEASE

0082364 BR-115164

********** DRIC U

********** DRIC Y

Reports quoted are not necessarily available to members of the public or to commercial organisations.

UNLIMITED

(1)

ROYAL AEROSPACE ESTABLISHMENT

Technical Report 90032

Received for prirting 26 June 1990

THE STEREOSCOPIC GEOMETRY OF THE REMOTE SENSING 'OPTICAL MAPPING INSTRUMENT'

by

N. S. Wells

SUMMARY

This Report examines the geometrical principles of stereoscopic remote sensing upon which the proposed Optical Mapping Instrument system is based. Consideration is given to the cartographic potential of the system in terms of constraints that arise from the viewing geometry, and conclusions are reached concerning the required accuracy and stability of the instrument.

Departmental Reference: Space 678

UNLIMITED

LIST OF CONTENTS

1 INTRODUCTION

The proposed **Optical Mapping Instrument** (OMI) is a space-based remote-sensing payload designed to produce high-resolution image data from which cartographic information can be derived. An outline specification of the OMI is given in Appendix A. The instrument has the capability of generating a stereoscopic pair of images of a given region, taken from different positions in a sun-synchronous, near-polar orbit. Northings and Eastings (or **planimetric data**) can be inferred from a single image, however the relative height of the terrain (or **topographic data**) is only derivable from a stereoscopic pair of images of the desired region. As examined in the present report, the **parallax**, *ie* the apparent relative displacement of features in the two images that results from a change in viewing position, is used to calculate the relative height of any point in the scene.

The main purpose of the Report is therefore to study the geometry associated with this stereo-viewing technique. The geometry has a direct bearing on the cartographic potential of the system since the desired system performance is governed by requirements arising from various geometrical constraints. Section 3 of this Report introduces the relationship between mapping potential and viewing geometry.

The imaging geometry is presented as a series of models of the physical situation, of increasing complexity. The initial approach to the problem, described in section 4.1, considers the target area on the Earth's surface as a stationary plane, with a single 'flagpole' representing an unknown relief height measured relative to the plane. The spherical Earth and circular OMI orbit are introduced in section 4.2, with section 4.3 presenting an analysis of Earth-rotation effects. The final discussion in section 4.4 briefly examines the consequences of treating the Earth as an oblate spheroid.

In any space-based imaging system the attitude control and measurement, and the pointing accuracy of the detectors, are fundamental design drivers since knowledge of these parameters is required during image processing and analysis. The basic requirements of the OMI are therefore examined in section 4.5.

2 GENERAL BACKGROUND

Accurate cartographic information of specific regions of the Earth's surface is of considerable value to many commercial, scientific and military users. Large areas of the world are however poorly mapped at relatively large scales *eg* 1:50000 scale, and therefore suitable information is often unavailable.

The use of a dedicated space-based stereoscopic system to provide the means of generating global cartographic data has long been recognised. In many respects it is simply a direct extension of the principles of aerial photography and photogrammetry used to obtain height information. A space-based platform does however maintain clear advantages over an airborne platform. These can include uniform detector velocity, high platform stability, and perhaps most importantly, the potential of rapid global coverage.

A number of technical problems, such as detector resolution, the design of the optics system, and the removal of geometric image distortions, must however be addressed before any satellite system can generate data suitable for mapping. The stringent cartographic requirements with which data must comply are discussed in the following section, and later in section 4.5.

Satellite concepts such as Stereosat[1] and Mapsat[2], were designed to exploit the benefits of stereo-imaging with the added potential of providing mapping data. These systems were however, abandoned for technical, political or economic reasons. Currently, the only 'commercial' example of a space-based remote sensing system capable of generating visible stereo-image pairs is the first in a series of CNES satellites, SPOT-1. This system, launched in 1986, is the first to validate the principle of deriving relief information from stereo-image pairs recorded by solid state linear array detectors aboard a dedicated orbiting platform.

3 STEREO-IMAGING AND CARTOGRAPHY

There are two basic solutions to the problem of achieving stereoscopic coverage of the Earth's surface by a space-based imager. One approach, as employed by SPOT-1, uses imaging systems which are designed to permit two observations of a desired area in different orbits and thereby generate a parallax between the two images. This is achieved by way of steerable mirrors that allow the field of view of the detectors to be tilted off-track, as shown in Fig 1.

The repeat cycle of the SPOT orbit is approximately 26 days, however, use of the across-track scanning facility can reduce the time between views, and hence allow a more rapid acquisition of the stereo-pair. Therefore, the **revisit capability** of the SPOT system is between 1 and 5 days, depending on the latitude. At 45° latitude SPOT can in principle image a target as frequently as 154 times a year, with a maximum panchromatic resolution of 10 m.

A major drawback of relying on different orbits to generate the necessary parallax between image-pairs, is that variables such as regional weather conditions can mean that suitable stereo-pairs are separated in time by weeks or

months. The co-registration of such images is often made difficult if the physical conditions applying to each image (*eg* scene illumination, atmospheric conditions, etc) have altered. For cartographic applications, the information content of the stereoscopic data may therefore be significantly reduced. These problems are most apparent when considering, for example, regions prone to frequent cloud cover or rapidly variable weather systems.

The alternative solution to the stereoscopy problem, involving fore-, aft- and nadir-viewing detectors, provides in theory a more convenient and practical method of generating stereo-images. As shown in Fig 2, the orientation of the telescopes (A, B and C), allows stereo coverage of a ground target (T) during a **single** orbit, and also provides the means of generating **stereo-image doublets** and/or **triplets**, thereby easing the task of image registration and target identification.

With this system, optical radiation from the Earth's surface is detected by solid state linear arrays of charge-coupled device elements placed at the focal planes of each of the telescopes. The **pushbroom** mode of operation is employed, ie continuous image scanning is achieved by using the 'forward' motion of the platform. This principle is presented schematically in Fig 3, for the case of a single nadir-viewing detector array. The orbital velocity of the platform v allows the detector to record a succession of image-strips, each of exposure, or **integration time** τ . After each integration period, the recorded data is electronically clocked out of the array into the instrument data handling system. The along-track resolution is therefore approximately given by the product of the platform's speed and the detector integration time.

The OMI system incorporates this type of design, and will provide the means of producing stereoscopic image data of very high resolution (nominally 5 m). The British Aerospace OMI feasibility study[3] has defined the baseline system parameters using RADARSAT as the host platform, and a relevant selection of these parameters are given in Table 1. Also included in the table is the equivalent data for SPOT-1, Mapsat and Stereosat[4].

Table 1

Specifications of OMI compared with those of other sun-synchronous, near-polar, stereo-imaging systems

	OMI	SPOT-1	Stereosat	Mapsat
Launch date	mid-late 1990s	1986	-	-
Nominal orbit height (km)	800	832	713	919
Pixel size (m)	5	10 or 20	15	10
Maximum off-nadir viewing	fore/aft ±24° x-track ±2.2°	x-track ±27°	fore/aft ±24° x-track ±2.5°	fore/aft ±23° x-track ±5.6°
Swath (km)	60	60	60	180
Repeat cycle (days)	11	26	48	18

The cross-track viewing angle of ±2.2° quoted for the OMI assumes that a cross-track scanning facility similar to that used in the SPOT HRV telescope system is not included in the design. However, if the OMI is to achieve complete global coverage, it is clear that such a system will be necessary for the following reason:

An orbital period of 100 minutes and a proposed repeat cycle of 11 days for the instrument dictates the minimum accessible swath width S that achieves total coverage, *ie*

$$S = \frac{2\pi R(\text{period})}{(\text{repeat time})} = 253 \text{ km}, \qquad (1)$$

where R is the equatorial Earth radius.

This does not however, allow for the Earth's rotation which, as demonstrated later in the Report, requires approximately 28 km of additional cross-track capability.

A minimum capability of approximately 280 km, combined with the desired ground resolution of 5 m, requires a total of 56000 pixels at the focal plane of each detector. A technical design limit of the order of 20000 pixels is currently considered optimistic[3], and therefore some form of mirror steering capability (to a maximum off-nadir angle of ±5°), is required if global coverage is to be achieved. It is recognised that under maximum off-nadir viewing

conditions the errors associated with loss of image focus and distortion of pixel shape will be enhanced, and this problem is addressed in section 4.2.

The need for very high ground resolution is predominantly a consequence of the requirements imposed by National Map Accuracy Standards (NMAS). These standards define the maximum allowable root mean square error in height (RMSE(z)) and plan (RMSE(x,y)) measurements, at a given map scale. The planimetric error is directly associated with the pixel size which, as demonstrated later in the report, in turn influences the error associated with heighting measurements.

The value of RMSE(z) is the total error in the heighting measurement of points in the image data, and as shown in Table 2, this value dictates the **contour interval** applicable to a particular map scale.

Table 2

Maximum allowable RMS errors for topographic maps meeting the requirements of the US NMAS[1]

Map scale	Planimetric RMSE(x,y)	Spot height RMSE(z)	Contour interval CI = 3.3 × RMSE(z)
1:500000	±150 m	±30 m	100 m
1:250000	±75 m	±15-30 m	50-100 m
1:100000	±30 m	±6-15 m	20-50 m
1:50000	±15 m	±6 m	20 m
1:25000	±7.5 m	±3 m	10 m

It is evident from Table 2 that for map scales of around 1:50000, the x, y and z errors attached to points in any image data must be constrained to the order of only several metres. An analysis of the viewing geometry is therefore of critical importance in determining the basic OMI system design, operation and data processing requirements.

4 GEOMETRICAL MODELS OF ALONG-TRACK STEREOSCOPY

The following sections deal with the analysis of the geometry of along-track stereoscopic imaging, and are presented as a series of models of the physical situation.

4.1 Model 1: The flat Earth.

The diagram in Fig 4 shows the simplest model of along-track stereoscopy in which the path taken by the detectors is parallel to a horizontal datum.

The point T in the figure represents relief at a height h above the datum, and the following discussion considers a stereo-image pair containing the point T , formed by fore- and aft-looking telescopes. The telescopes are shown schematically as two cameras of focal length f at an altitude H , with the flight direction drawn from left to right. Any displacement measured in the flight direction is regarded as a positive quantity.

The displacements of the point T , measured in the image planes of the cameras with respect to the image centres, are d and -d' respectively.

By similar triangles:

$$\frac{f}{d} = \frac{H - h}{x} , \tag{2}$$

where x is the displacement of the sub-satellite point to the object. The displacement of T in the image plane, measured relative to the image centre of the fore-looking camera is therefore

$$d = \frac{xf}{H - h} . \tag{3}$$

Similarly,

$$-d' = -\frac{x'f}{H - h} . \tag{4}$$

For any stereo-pair of images, the **base** B is defined as the separation of the two lens positions at the instants when the photographs were taken. Therefore

$$B = x - x' , \tag{5}$$

since a stereo-pair may be generated when the displacement d' is positive and $d' < d$. With reference to the figure,

$$B = x + x' \tag{6}$$

As defined in section 1, the measured parallax p is the apparent, relative displacement of features in the two images that results from the change in viewing position. Therefore the parallax between the positions of the point T in the image-pair is

$$p = d - (-d') = \frac{Bf}{H - h}, \tag{7}$$

and thus the unknown height h is given by

$$h = H - \frac{Bf}{p} . \tag{8}$$

Equation (8) is valid for a height h at any position along the ground swath perpendicular to the ground track, since all points along this line have the same value of parallax p.

The uncertainty in the measurement of h, as a function of parallax measurement accuracy may be found by differentiating (8) with respect to p:

$$\frac{dh}{dp} = \frac{Bf}{p^2} . \tag{9}$$

Substituting for p:

$$\frac{dh}{dp} = \frac{(H - h)^2}{Bf} . \tag{10}$$

Since $H >> h$, and the measured quantity p is discrete rather than continuous, equation (10) becomes

$$\delta h = \frac{\delta p H^2}{Bf} . \tag{11}$$

Rewriting (11):

$$\delta h = \frac{H/f \delta p}{B/H} . \tag{12}$$

The ratio H/f defines the scale of the image at the focal plane. If for example, the altitude of the platform is increased, then for a given focal length of telescope, the image scale increases.

The denominator of (12) is the so called **base-to-height ratio** that is used extensively in stereoscopic aerial photography. As predicted by (12), the heighting error δh is inversely proportional to the B/H ratio, for a given parallax measurement error δp, and therefore a B/H value is often used to indicate the height accuracy properties of a given stereo-pair. Reduced

heighting error is favoured by greater B/H ratios, *ie* reduced altitude and increased separation of viewing positions.

The relationships between the B/H ratio and δh, for different values of parallax measurement error δp are presented in Fig 5. Since the error in parallax measurement is most conveniently expressed in terms of pixels or fractions of pixels, equation (12) indicates that a flat, extended target may have a measurement accuracy of 0.5 pixels and therefore $\delta p = 0.7$. The shallowest curve in Fig 5 is for the case of a large target which is measurable to a high degree of accuracy, *eg* $\delta p = 0.2$.

If a heighting error of, for example, less than 2 pixels is required, the figure indicates that it is necessary to record the image data at B/H ratios of greater than approximately 0.6. Comparatively large values of B/H (*eg* 1.4), although desirable for reducing δh, can generate problems such as extreme vertical exaggeration of the image data or at worst, regions of image shadowing. A ratio of between 0.5 and 1 is usually considered desirable, and is often designed for.

If the fore and aft viewing angles, measured with respect to the vertical, are chosen to be equal, a B/H of unity dictates the offset angle at which the telescopes must be held since this is given by $\arctan(1/2) \approx 26° 34'$. Similarly, if B/H is to be 0.5 then the required offset to the vertical is 14° 2'.

As a specific example of the difference between these design options, consider the parallax error for a point target referred to earlier: $\delta p = 1.4$. A base-to-height ratio of one implies a target height error of about ±7 m, whereas $B/H = 0.5$ generates an error of ±14 m.

The geometry of Fig 4 is such that the dimensions B and H must be negligible compared to the radius of curvature of the Earth. This assumption is applicable to most instances of aerial photography, but the additional relief displacement produced by surface curvature requires correction when imaging at orbital altitudes. As depicted schematically in Fig 6, the concept of base and height measurements also has to be modified. The situation of $B/H = 1$ is shown, *ie* $FG/EF = 1$. The fore and aft viewing positions for a certain target area are the points A and D and therefore the actual $B/H = BC/AB > 1$ The additional relief displacement at the target is represented by the separation of BC and FG .

The proposed OMI altitude of about 800 km, combined with the need for very high topographic accuracy, implies that the effect of the Earth's curvature must be included in a discussion of the viewing geometry.

4.2 Model 2: The spherical Earth.

Consider the platform moving in a circular orbit of altitude H', as presented in Fig 7. The point T is at a height h above a co-planar, circular datum of radius R, and is imaged by the fore and aft detectors at the orbital points M and N. The base and height of the system are now redefined as the distances MN and OP respectively. It is assumed that the fore and aft telescopes (of focal length f), are mounted at equal angles to the nadir ie the magnitude of the relative displacement of the point T in the image plane is the same for each telescope.

Therefore, by similar triangles, the parallax

$$p = \frac{2fx}{H' + y}, \tag{13}$$

where x and y are defined in the figure.

The cosine of μ gives the result

$$\cos(\mu) = \frac{R - y}{R + h} = \frac{R + H}{R + H'}, \tag{14}$$

and therefore,

$$y = R - \frac{(R + H)(R + h)}{(R + H')}. \tag{15}$$

The unknown distance x in equation (13) is similarly found:

$$\sin(\mu) = \frac{x}{R + h} = \frac{B}{2(R + H')}, \tag{16}$$

and hence,

$$x = \frac{B(R + h)}{2(R + H')}, \tag{17}$$

and the substitution of (15) and (17) into (13) gives an expression for the total measured parallax:

$$p = \frac{Bf(R + h)}{(R + H')^2 - (R + h)(R + H)}. \tag{18}$$

Equation (18) may be rearranged to give the unknown height h in terms of measurable or known quantities:

$$h = \frac{p(H'^2 + 2H'R - HR) - fBR}{p(R + H) + Bf} . \tag{19}$$

Since it is desirable to know the error with which h is measured, equation (18) is now differentiated by using the following law:

$$\frac{d}{dx}\left\{\frac{u(x)}{v(x)}\right\} = \frac{vdu/dx - udv/dx}{v^2} . \tag{20}$$

Let

$$u(h) = Bf(R + h) , \tag{21}$$

and

$$v(h) = (R + H')^2 - (R + h)(R + H) . \tag{22}$$

Therefore, using (20),

$$\frac{dp}{dh} = \frac{\{(R + H')^2 - (R + h)(R + H)\}Bf + Bf(R + h)(R + H)}{\{(R + H')^2 - (R + h)(R + H)\}^2} , \tag{23}$$

which is rearranged to give

$$\frac{dh}{dp} = \frac{\{(R + H')^2 - (R + h)(R + H)\}^2}{Bf(R + H')^2} , \tag{24}$$

and if it is again recognised that h and p are discretely measured quantities, as was noted in the derivation of (12),

$$\delta h \approx \frac{\{H'(2R + H') - RH\}^2 \delta p}{Bf(R + H')^2} , \tag{25}$$

assuming that $h << R$.

If in (25), the radius R is allowed to approach infinity, (ie the geometric model tends towards the 'flat Earth' situation of the previous section), then since

$$\lim_{R\to\infty} (H') = H , \tag{26}$$

$$\lim_{R\to\infty} (\delta h) = \frac{H^2 \delta p}{Bf} , \tag{27}$$

which is consistent with equation (11).

Fig 8a shows part of Fig 7 in more detail, but with the object height set to zero. The diagram shows the fore-looking situation with the forward range r to the plane again shown at a fixed angle Φ to the sub-satellite point N.

Due to the curvature of the Earth, the telescope offset angle Φ is now given by

$$\Phi = \arcsin\left\{ \frac{R \sin(\phi)}{(R + H')} \right\} , \tag{28}$$

where ϕ is shown in the figure, and is known from

$$\phi = \arcsin\left\{ \pi - \frac{B}{2r} \right\} , \tag{29}$$

with

$$r = \sqrt{\{ (B/2)^2 + H^2 \}} . \tag{30}$$

For the case when $B/H = 1$, equation (30) reduces to

$$r = \frac{B\sqrt{5}}{2} , \tag{31}$$

and the angle Φ is found from (28) to be 23° 25', (*cf* 26° 34' if the Earth's surface is regarded as flat). This more accurate value is used throughout the remainder of this section.

If a telescope identical to that used for the nadir view (*ie* f = 1.12 m), is used for the fore and aft observations, the image pixel size will be increased. This implies a loss of resolution or focus. Therefore the focal length of these telescopes must be suitably increased to accommodate for the fact that $r > H'$. For 5 m pixels to be realised at the ground, the new focal length is calculated to be 1.24 m.

It is of interest to evaluate the increase in pixel dimensions for 5 m resolution nadir due to the effect of the Earth's curvature. The pixel to pixel variation is small across the nominal swath of 60 km centred on the ground track, however the effect is pronounced when the swath is steered across-track by the proposed pointing mirror. This effect is now considered.

If the nadir swath is steered through a cross-track angle Γ, as shown in Fig 8b, the cross-track pixel length, $a + b$ can be assumed to lie in the tangential plane to the Earth's surface at the point where the range r' intersects the surface.

In order to calculate the pixel length $a + b$ it is necessary to derive expressions for the angles Σ, Σ_1 and Σ_2 .

Applying the Sine Rule to the system gives the angle subtended at the centre of the Earth

$$\Sigma = \arcsin\left\{\frac{(R + H')\sin(\Gamma)}{R}\right\} - \Gamma. \tag{32}$$

Similarly

$$\frac{\sin\left(\Gamma - \Gamma_1 + \Sigma - \Sigma_1\right)}{R + H'} = \frac{\sin(\Gamma - \Gamma_1)}{R}, \tag{33}$$

where Γ_1 is the half-angle subtended by the nominal 5m pixel at the nadir, *ie*

$$\Gamma_1 = \arctan\left\{\frac{2.5}{8 \times 10^5}\right\} \approx 1.8 \times 10^{-4^\circ} . \tag{34}$$

Equation (33) rearranged gives

$$\Sigma_1 = \Gamma + \Sigma - \Gamma_1 - \arcsin\left\{\frac{(R + H')\sin(\Gamma - \Gamma_1)}{R}\right\} = \arctan\left(\frac{a}{R}\right) . \tag{35}$$

Similarly

$$\Sigma_2 = \arcsin\left\{\frac{(R + H')\sin(\Gamma + \Gamma_1)}{R}\right\} - \Gamma - \Gamma_1 - \Sigma = \arctan\left(\frac{b}{R}\right) . \tag{36}$$

Therefore the length of the pixel is now known from the combination of equations (35) and (36).

A plot of pixel length $a + b$ versus cross-track angle Σ is presented in Fig 9. It is evident that the dimensional increase of the nominal pixel is a serious effect at even relatively modest cross-track look angles.

The effect of treating the Earth's surface as spherical as opposed to planar may also be readily appreciated by considering the difference between the expressions for the heighting measurement error δh derived for the 'flat' and 'curved' cases, (equations (11) and (25) respectively). Since the definition of the base B in the two situations is different let (11) be rewritten as

$$\delta h \approx \frac{H'^2 \delta p}{B_1 f} = k_1 \delta p \ , \tag{37}$$

($H = H'$ for the 'flat Earth' model), and (25) as

$$\delta h \approx \frac{\{H'(2R + H') - RH\}^2 \, \delta p}{B_2 f (R + H')^2} = k_2 \delta p, \tag{38}$$

where

$$B_1 = H' = 800.0 \text{ km} \ , \tag{39}$$

and

$$B_2 = H \ , \tag{40}$$

for base-to-height ratios of one.

In order that B_2 may be evaluated, H and μ must be calculated.

From the geometry of Fig 8a,

$$\mu = \arcsin \left\{ \frac{\sin(\Phi)(R + H')}{R} \right\} - \Phi = 3^\circ \, 9' \ , \tag{41}$$

and

$$H = \{(R + H') \cos(\mu)\} - R = 789.13 \text{ km} \ . \tag{42}$$

Therefore $B_2 = 789.13$ km and the constants k_1 and k_2 may now be quantified. It is found that

$$k_1 \approx 1.1 k_2 \ . \tag{43}$$

This indicates that with respect to the planar model, Earth curvature causes a reduction in the heighting measurement error of about 10%. The graph in Fig 10 is a plot of equation (25) as a function of B/H for the three values of parallax measurement error δp considered in Fig 5. If the curves in Fig 10 are compared with those in Fig 5, the 10% reduction in δh is apparent.

This section has quantified the effects associated with the curvature of the Earth but has not addressed the fact that along-track stereo-coverage is a function of time. Any perturbations of the imaging system during the time required to record image data will, as a result, be translated into horizontal and vertical distortions of the data.

The following effects must therefore be determined and suitably compensated for:

(i) The rotation of the Earth.
(ii) Platform stability, attitude and rate errors.
(iii) Altitude perturbations and the non-spherical nature of the Earth.
(iv) Mechanical and thermal instabilities within the instrument.

The scope of the present study implies that only the first three of the above problems are examined in this Report.

4.3 Model 3: The rotating Earth

The following section addresses the problem of Earth rotation in respect of the fore-/aft-viewing situation, since this is where the effect will be most problematic. Fig 11 depicts a model identical to that described in section 4.1 except that the unknown object (of height h), moves with a constant velocity across the OMI ground-track between the fore and aft observations, thereby simulating Earth rotation. The time taken for the satellite to move from X to Y along the flight line is the same as that for the object to move from S to T. The dotted lines MN and OP in the figure represent the respective viewing lines of the fore- and aft-looking telescopes.

This is a convenient way of examining the situation since it allows the use of many of the parameters included in the preceding sections of this Report, and hence a direct comparison between the different models may be drawn. The analysis is somewhat simplified by neglecting the effects of Earth and orbit curvature.

The parallax p associated with the target will be treated in terms of perpendicular components in the image plane, p_x and p_y, since p is no longer constrained to a single axis (*cf* section 4.1). Distances d_1 and d_2 are the

positions of the top of the object, relative to the image centre, measured in the image plane.

By similar triangles,

$$d_1 = \frac{fH \tan(\Phi)}{(H - h) \cos(\alpha)} \tag{44}$$

and

$$d_2 = \frac{fH \tan(\Phi)}{(H - h) \cos(\beta)} , \tag{45}$$

where α and β are given in the figure and Φ is the angle between the local vertical and the line from the telescope to the object.

The total parallax in the x- and y-directions is respectively

$$p_x = d_1 \cos(\alpha) + d_2 \cos(\beta) , \tag{46}$$

and

$$p_y = d_1 \sin(\alpha) + d_2 \sin(\beta) . \tag{47}$$

Therefore

$$p_x = \frac{2fH \tan(\Phi)}{H - h} = \frac{Bf}{H - h} , \tag{48}$$

and

$$p_y = \frac{f(L_1 + L_2)}{(H - h)} , \tag{49}$$

where $L_1 + L_2$ is the total distance moved by the object, perpendicular to the ground track, as shown in Fig 11, and B is the base of the system as defined in section 4.1.

The parallax of the object is therefore

$$p = \sqrt{\{p_x^2 + p_y^2\}} = \frac{f}{H - h} \sqrt{\{B^2 + (L_1 + L_2)^2\}} \tag{50}$$

Let the velocity of the satellite be v_s and the velocity of the object be v_o, at an angle θ to the ground track, as shown in Fig 12. Then

$$L_1 + L_2 = \frac{Bv_o \sin(\theta)}{v_s - \{v_o \cos(\theta)\}} , \tag{51}$$

and (50) becomes

$$p = \frac{Bf}{(H - h)} \sqrt{1 + \left\{ \frac{v_o \sin(\theta)}{(v_s - v_o \cos(\theta))} \right\}^2} \quad . \tag{52}$$

Differentiation of (52), including the assumption that $H - h \approx H$, gives

$$\delta h \approx \frac{H^2}{Bf} \left\{ 1 + \left\{ \frac{v_o \sin(\theta)}{(v_s - v_o \cos(\theta))} \right\}^2 \right\}^{-1} \delta p \ , \tag{53}$$

for the error in the measurement of the height h. This is consistent with equation (11) if $v_o = 0$. The square root term in (53) is a maximum at the equator where $v_o = 0.46$ km/s . Therefore the maximum decrease in the heighting error for the sun-synchronous orbit ($\theta = 98°$), due to the motion of the target is approximately 4%.

From the right-angled triangle containing $L_1 + L_2$:

$$L_1 + L_2 = v_o t \sin(\theta) \ , \tag{54}$$

where t is the time between the fore and aft views.

Equation (54) may be used to estimate the magnitude of the across-track displacement of the object for a given v_o and θ. The time t must be less than approximately 120 s since this is the time between views for the case when the velocity $v_o = 0$. For the worst case, *ie* a target on the equator, it is found that

$$L_1 + L_2 \approx 55 \text{ km} \ . \tag{55}$$

Since the OMI swath is 60 km wide, it is evident that only 9% of equatorial targets recorded in the fore-looking view will be stereoscopically recorded by the aft telescope. This undesirable situation clearly represents a major design driver and can be alleviated by 'yaw steering'. This involves active control of the yaw angle of the imaging system such that a target observed by the n^{th} pixel in the image line of the fore-looking telescope is also observed by the n^{th} pixel in the aft-looking telescope. The idea of yaw steering was recommended in the proposed operation of Stereosat[1] and involved dynamic control of the platform's orientation. Accurate platform yaw control is, however, technically demanding

and can be operationally inconvenient. Yaw steering of mirrors mounted within the optical trains of both telescopes is perhaps the most satisfactory solution since this method does not present undue technical and operational problems. This notion will now be considered for the OMI system.

The yaw steering technique is shown in Fig 12, which is simply a plan view of Fig 11 with the required yaw angle given by Y_a . A target at point S is observed in the centre of the fore-looking image line MN , and is later observed at T which is the centre of the aft-looking image line OP . By steering the system in this manner the parallax of the target in the cross-track direction is zero, (cf the discussion associated with Fig 11).

For simplicity it can be arranged so that the mirrors in both telecopes are orientated to achieve the same angle Y_a either side of the line of flight.

It is found that

$$\tan Y_a = \frac{R\Omega_e\sqrt{\{\cos^2(L) - \cos^2(i)\}}}{v_s - \{R\Omega_e \cos(i)\}} , \qquad (56)$$

and the rate of change of yaw angle with time t is given by

$$\frac{dY_a}{dt} = \frac{R\Omega_e\Omega_s \sin(i) \sin(\Omega_s t)/\{v_s - (R\Omega_e \cos(i))\}}{1 + \left\{R\Omega_e \sin(i) \cos(\Omega_s t)/(v_s - (R\Omega_e \cos(i)))\right\}^2} , \qquad (57)$$

where L = latitude of sub-satellite point,

Ω_e = angular velocity of the Earth $\approx 4.17 \times 10^{-3}$°/s,

Ω_s = angular velocity of sub-satellite point ≈ 0.06°/s,

i = orbit inclination ≈ 98°.

The derivation of (56) and (57) is given in Appendix B.

A plot of yaw angle versus latitude, derived from equation (56), is shown in Fig 13. The graph is drawn for half an orbit, ie from pole to pole. As anticipated, the required yaw angle is a maximum (3° 52') over the equator, and zero at the maximum latitude of the sub-satellite point (82°).

Fig 14 is a plot of (4.56) and shows the rate of change of yaw angle over one orbit, with t = 0 corresponding to the sub-satellite point passing over the equator. The maximum angular rate of a steerable mirror is seen to be no more than 15 arcsec/s. Assuming that such a system could be controlled by a simple

on-board algorithm, it therefore appears to represent a practical solution to the problem of target movement between views.

It is also recognised that steerable mirrors significantly increase the probability of obtaining cloud-free stereo-pairs and, as noted earlier, also ensure that the OMI has a complete global coverage capability.

4.4 Model 4: The oblate spheroid

This section examines briefly the consequences of the fact that the Earth's surface is more accurately modelled by an oblate spheroid rather than a true sphere.

Fig 15 depicts a 'circular' and 'elliptical' Earth cross-section, together with the satellite at the point S . The centre of the Earth is at the origin of the figure, and the x-y plane is oriented such that the nodal line of the orbit lies along the z-axis.

It is apparent from the figure that the influence of a non-spherical surface on image scale, (and the swath area coverage), increases with satellite latitude L . The maximum error associated with the cross-track variation of area coverage will therefore occur at the lateral margin of the image (angle e from the local vertical), when the latitude of the satellite is a maximum. This is the condition depicted in the figure.

In Cartesian coordinates, the elliptical cross-section whose semi-major axis is defined by the radius R of the spherical datum, is described by

$$\frac{x^2}{R^2} + \frac{y^2}{b^2} = 1 \ , \tag{58}$$

and the respective equations of the lines TS and NS in the figure are

$$y = x \tan(L - \varepsilon) + \frac{(R + H) \sin(\varepsilon)}{\cos(L - \varepsilon)} \ , \tag{59}$$

and

$$y = x \tan(L) \ . \tag{60}$$

The combination of (58) with (59) and (60) leads to the coordinates of the sub-satellite point N and the observed cross-track point T . The relative increase in the cross-track coverage due to the elliptic rather than circular curvature is then deducible.

The semi-minor axis b is assumed to be the measured polar radius of the Earth, *ie* 6357 km, and the maximum values of L and ε for the OMI, are 82° and 2° 9' (with no off-track scanning), respectively. Therefore, with respect to the true sphere, the maximum cross-track increase in ground coverage due to oblateness is calculated to be about 900 m, or 180 pixels. This corresponds to an increase over the 'planar' swath of approximately 1% .

It is also noted that a similar calculation for the fore-looking case suggests that the along-track increase due to an elliptical rather than a spherical surface, will be of the order of 6.5 km (maximum).

This disparity, like earlier considerations of how the true viewing geometry quantitatively differs from the desired planar representation of the Earth's surface, may generate correlation problems. It is recognised that the majority of the geometric distortions discussed are, in theory, rectifiable only to the accuracy with which the satellite altitude, position and orientation are known.

4.5 Attitude, position and pointing control

If consideration is given to a circular satellite orbit, it is therefore assumed that the detector altitude is invariant. In practice however, finite perturbations of the satellite orbit are generated by, for example, the non-uniform geopotential and solar radiation pressure. The consequence of these effects is to cause fluctuations in the satellite altitude and orientation, which for the OMI would directly alter the scale (and focus) of the data, and therefore constitute a time-varying geometric error.

Any perturbation of the detection system during the time interval required for stereo-imaging will also cause correlation difficulties between stereo-pairs. Therefore the roll, pitch and yaw movements of the platform, which will cause deformations of the nominal image, will demand adequate control and measurement via on board sensors, and accurate correction during ground processing. Only in this way will useful, cartographic data be compiled.

In practice, the transformation of image data into a defined ground coordinate system usually dictates the use of a number of ground control points (GCPs). GCPs are prominent features in the image scene with accurately known coordinates, (*eg* road or river intersections), that serve as points of reference for the image data. In well mapped parts of the world, the geometric correction of an image is often simplified by the presence of many GCPs, each with errors in X, Y and Z coordinates of a few metres.

The absence of ground control in many poorly mapped locations (where the OMI data will doubtless be of greatest value), implies that the attitude and position of the instrument has to be recoverable by alternative means. If precise altitude information is not attainable then it is clear that although relative spot heights may be known to within ±10 m, the absolute topographic accuracy of the data may be unknown, or at best known to only several hundred metres.

Absolute position information may be achieved directly by way of an on-board altimeter or by a separate means such as information derived from the Navstar Global Positioning System (GPS). This latter method, which is due to become fully operational in the 1990s, will consist of up to 18 satellites in various 12 hour orbits continuously providing an instantaneous positional accuracy of ±5-15 m for any spacecraft equipped with a suitable receiver[5]. The GPS may also be used to derive satellite velocity information to the order of ±1 m/s.

As discussed with respect to Stereosat[1], one approach to solving the problem of little or no ground control involves the recording of system status information into the image data. For the OMI it may be feasible to use the first several pixels of each image line to store relevant 'house-keeping' data, with a number of successive lines being used to record all the necessary information. Once the data from the appropriate on-board sensors has been registered, the process then repeats continuously so that the beginning of every image line contains a few bytes of system data. This data may include attitude and angular rate information, the system clock time and perhaps altimeter measurements. Suitable ground processing may then be employed to retrieve this data and use it to orientate and correct the images received.

The present section examines the accuracy with which this information must be known, and also the extent to which the platform must be controlled. In order that some initial conclusions may be reached, consideration is given to the 'planar' viewing geometry presented first in section 4.1.

Fig 16 illustrates the general concept of a pointing error by considering the aft-looking detector imaging at a deflected angle Φ' to the vertical, rather than the correct angle Φ. An expression for the induced heighting error δz can be determined by considering triangle acd, in the figure:

$$bd = H\{ 1 - \tan(\Phi) \cot(\Phi') \} , \tag{61}$$

and

$$cd = \delta z \sec(\Phi) . \tag{62}$$

Also,

$$\frac{\sin(\Phi')}{cd} = \frac{\sin(\Phi + \Phi')}{bd} \quad . \tag{63}$$

The substitution of (61) and (62) into (63) gives the result :

$$\delta z = \frac{H\{\tan(\Phi') - \tan(\Phi)\}}{\tan(\Phi') + \tan(\Phi)} \quad , \tag{64}$$

where, in terms of the associated planimetric error δx,

$$\delta z = \delta x \cot(\Phi) \quad . \tag{65}$$

The relative spot height accuracy δz given by (64) is only one term in the expression for the total root mean square error in heighting measurement RMSE(z), which was introduced in section 3. Therefore

$$\text{RMSE}(z) = \sqrt{\{(\delta z)^2 + (\delta_1)^2 + (\delta_2)^2 + \ldots\}} \quad , \tag{66}$$

where δ_1, δ_2 , etc are the geometric errors associated with, for example, the optics, focal plane and data processing techniques.

Many of these additional uncertainties are difficult to evaluate precisely in view of the absence of information concerning system designs. Therefore, in the following analysis, the assumption is made that the most significant term in (66) is the pointing error of the telescopes, *ie* RMSE(z) and δz are equivalent. The resulting conclusions therefore indicate the maximum cartographic potential of the system.

With reference to Fig 17, it is again evident that B/H ratios of the order of 0.6 and larger are required by a cartographic system that demands the minimum of vertical displacement errors. The figure shows the graphical relationship of δz and B/H ratio for various pixel values of δx , and also indicates the importance of reducing the along-track error δx to less than one pixel. If, for example, the value of δx is one pixel for 5 m image data recorded at B/H = 1 , then the associated spot height accuracies will be ±10 m.

The cartographic requirements of the US NMAS presented in section 3, indicate that this may correspond to a topographic contour interval, CI , of only 50 m since

$$CI = 3.3\ RMSE(z) \ . \tag{67}$$

With respect to the OMI, a planimetric error $\delta x = 2.5$ m (*ie* a half pixel) dictates $\delta z = 4.9$ m, and equation (64) in turn defines the maximum allowable deflection error of the detectors, $\Phi' - \Phi$, calculable from:

$$\tan(\Phi') = \frac{(H + \delta z)\ \tan(\Phi)}{(H - \delta z)} \ . \tag{68}$$

In the case of fore/aft stereoscopy, this deflection is found to be approximately 2.5×10^{-4}°, and therefore constitutes the minimum (desirable) attitude knowledge requirement of the system, for a planimetric error of half a pixel. If knowledge to this accuracy is available from the platform, then the requirements on the platform attitude control system (ACS), are less stringent and only depend on the desired targeting accuracy of the instrument. For example, to ensure that the OMI is targeted to within about ±200 m of a ground point, the ACS must be accurate to approximately 15×10^{-3}°.

Table 3 summarises the results of this section and also lists the current specifications for the RADARSAT platform ACS. With reference to the attitude control and knowledge data, it is evident that the platform ACS will not meet the OMI requirement for a half pixel error at any point in any image. In order that 5 m resolution is not compromised or ground processing procedures greatly increased it may therefore become necessary to have at least one GCP in any given image.

If the platform did not suffer from rotation rate errors, a single GCP could correct a large number of images along the ground track and as such would not reduce the mapping capability of the instrument. However, as discussed below, the presence of angular rate errors suggest that some form of GCP sampling will be required.

During the integration of a single image line, the platform angular rate errors must be sufficiently small to prevent the 'smearing' of adjacent ground pixels. If it is assumed that the smearing effect will not occur as long as the relative displacement of the image line is constrained to be less than half a pixel at the ground during the 0.75 ms image integration time, this implies that

the angular motion of the detectors must be less than about 0.2°/s, about any axis. Smearing of image points will also occur as a result of the transfer functions of the optics and detectors, however half a pixel is chosen here to give a coarse indication of the platform control requirements.

More demanding angular rate control is clearly required during the formation of a complete single image (≈ 60 km × 60 km), since for the OMI this will require almost 9 s of continuous imaging time. In this case, a half pixel error across the entire image dictates along- and across-track rotation rate control accurate to about 2×10^{-5}°/s, which is about 30 times less than the performance of the SPOT-1 ACS. If this control level can be achieved, the result is a system which generates single images that require no geometric correction for platform angular rate errors. With reference to Table 3, the angular rate control quoted for RADARSAT suggests that a single image will suffer a distortion or 'smearing' of more than 2.5 pixels, which is likely to be unacceptable for 1:50000 scale mapping applications.

Table 3

Summary of the attitude and angular rate requirements of the OMI and a comparison with the RADARSAT platform specifications

	Single image	Fore/aft pair	RADARSAT specification
Attitude control ($\times 10^{-3}$°)	15	15	40
Attitude knowledge ($\times 10^{-3}$°)	0.25	0.25	30
Rate control ($\times 10^{-5}$°/s)	2	0.1	10
Rate knowledge ($\times 10^{-5}$°/s)	2	0.1	3

The problem of angular rate control and determination is greatest when considering the time interval between the fore and aft detectors recording the same scene (approximately 123 s). For example, a reduction in image-pair overlap of almost 30 km (half the nominal swath) occurs if the cross-track angular rate exceeds about 17×10^{-3}°/s. Indeed, a point coordinate error of only half a pixel between compatible fore and aft images requires cross-track angular rate control of the order of 1×10^{-6}°/s. Mechanical control to this latter order is

not attainable using current angular rate control devices and as recorded in Table 3, RADARSAT angular rate control is two orders of magnitude worse than this. It is apparent therefore that at least one GCP will be required to correctly position a stereo-pair, assuming the single images are correct in themselves.

Since control is not possible, then it is necessary to measure the rotation rates to the accuracies stated above. Again however, the platform is incapable of achieving these measurements and therefore suitable angular rate measurement devices will have to be incorporated into the OMI design, independent of the RADARSAT platform systems. Fluid-loop, inertial angular displacement sensors currently available for space applications, combined with standard gyroscopic packages or star sensors, may satisfy this requirement.

It should be noted that control to the sort of levels discussed for stereo-pairs is not imperative for the successful co-registration of targets in the two images. The angular rate stability over the 123 s interval is dictated by the maximum extent to which the reduction in stereo-pair overlap may be tolerated, assuming that each of the images are distortion-free in themselves. If for example the angular rate measurement is assumed to be possible to about a value of 1×10^{-4}°/s, then the maximum target coordinate error of the pair is of the order of 50 pixels. The successful correlation of a stereo-pair would be achieved by means of a single GCP, present in both scenes.

The results presented in this section are not intended to be an exhaustive and thorough treatment of the problems associated with attitude control and determination, but are for use as indicators of the required system performance. It is evident that if the OMI data is to be used for large scale topographic maps then angular rate and pointing accuracies will dictate the use of very high precision on-board sensors and/or controllers, and sophisticated data processing techniques.

5 CONCLUSIONS

The OMI is proposed as a means of generating continuous, high resolution stereoscopic image data, from which cartographic information may be derived. The basic system design allows image data to be collected in the along-track direction by fore-, aft- and nadir-viewing linear array detectors. The instrument will be configured for a nominal ground swath width of 60 km with a pixel size of 5 m. Over the short time period required to record the image of a ground target in both the fore and aft detectors, the physical conditions that apply to the

target area will be unaltered. In principle therefore, this method of stereoscopy allows the simple and comparatively rapid registration of high resolution stereo-pairs and stereo-triplets.

Of the various user disciplines, cartography places the greatest demands on the system design parameters. The completeness and accuracy requirements of cartographic standards also dictates the degree of error compensation required. The accuracy of the final image is largely a function of sensor control and attitude determination, and it is concluded that if the relief measurement accuracy of the instrument is to be compatible with a 1:50000 scale map, the following specifications must be realised:

(i) Control of the instrument attitude to the order of 15×10^{-3}°, thereby allowing a reasonable targeting accuracy of a few hundred metres.

(ii) Recovery of the sensor attitude to about 2×10^{-4}° to maintain the geometric accuracy of each image at ±0.5 pixel.

(iii) Knowledge of the platform angular rate errors to better than 2×10^{-5}°/s is desirable for the reason given in (ii), and if possible to about 1×10^{-6}°/s for maximum fidelity of a stereo-image pair.

The consequences of the above on the system design and operation include the following:

(i) The incorporation of on-board attitude sensor data into the OMI data stream in order that for any given image, the orientation of the detectors may be accurately recovered.

(ii) The use of 'remotely-sited' sources of position information, such as altimeters, the Navstar GPS or ground control points to aid image rectification and processing.

In view of the size of the swath of the instrument, and the nominal orbit characteristics, it is recognised that the optics design could include steerable mirrors and thereby allow rapid and complete global coverage, together with improved probability of cloud-free target acquisition. These mirrors may be used in a 'yaw steering' role in order that the problems associated with Earth rotation may be offset.

As outlined in this Report, there exist various challenging geometrical requirements on the OMI system which must be met if the instrument is to fulfil its primary function with the desired capability. Assuming that 1:50,000 topographic maps of scenes containing little ground control can be compiled from an operational OMI, then it is not inconceivable that larger scales may be produced

or at least updated. On this basis, it is expected that the cartographic potential of the OMI will prove to be of considerable value to a wide variety of users within the Earth observation community.

Appendix A

AN OUTLINE SPECIFICATION FOR THE OMI

The following data is an outline specification for the OMI[3]. These criteria form the basis of the work presented in this Report.

A.1 The host platform is RADARSAT in an 800 km, circular, sun-synchronous, near-polar orbit.

A.2 Along-track stereoscopic capability is provided by two identical compact Schmidt telescopes.

A.3 Each telescope has an aperture of ≈400 mm and an optical train which corrects and focuses the incident light field onto a Focal Plane Assembly (FPA).

A.4 The FPA contains the primary and secondary function sensors. The primary (5 m mapping) function is a redundant pair of linear array charge-coupled devices (CCD) that generate digital count outputs in response to the incident light, in the NIR band (0.7 to 1.0μ). The secondary functions may include further CCDs to provide a very high resolution patch, and multispectral capabilities.

A.5 Telescope viewing angles of ±24° give a base:height ratio of ≈1.0.

A.6 An across-track capability to ±20° may be achieved by way of a steerable mirror, mounted at the aperture of each telescope. These will allow complete global coverage of the instrument from the proposed orbit. This facility also allows for frequent attempts at data-taking.

A.7 The swath width is 60 km.

A.8 Each image line consists of 12000 square pixels, each 5 m × 5 m on the ground.

Appendix B

GEOMETRIC ANALYSIS OF THE 'YAW STEERING' TECHNIQUE
(see section 4.3)

The distance represented by the line ST in Fig 12 is equal to the velocity v_o multiplied by the time t between the fore and aft views. Therefore, applying the Sine Rule to the triangle SNX in the figure gives

$$\frac{\sin(Y_a)}{v_o t/2} = \frac{\sin(\theta)}{B/2}, \qquad \text{(B-1)}$$

and therefore the time taken is given by

$$t = \frac{B \sin(Y_a)}{v_o \sin(\theta)}. \qquad \text{(B-2)}$$

The distance XY in the figure is given by

$$v_s t = B \cos(Y_a) + v_o t \cos(\theta), \qquad \text{(B-3)}$$

and hence

$$t = \frac{B \cos(Y_a)}{v_s - \{v_o \cos(\theta)\}}. \qquad \text{(B-4)}$$

Combining (B-2) and (B-4):

$$\tan(Y_a) = \frac{v_o \sin(\theta)}{vs - \{v_o \cos(\theta)\}}. \qquad \text{(B-5)}$$

Fig 18 shows the sun-synchronous OMI orbit projected onto a spherical Earth's surface. The sub-satellite point s is at a latitude L . Spherical triangle trigonometry, applied to triangle snm gives the result

$$\cos(\theta) = \frac{\cos(i)}{\cos(L)}. \qquad \text{(B-6)}$$

The latitude-dependent velocity of the target

$$v_o = R\Omega_e \cos(L), \qquad \text{(B-7)}$$

and the combination of (B-6) and (B-7) with (B-5) gives

$$\tan(Y_a) = \frac{R\Omega_e\sqrt{\{\cos^2(L) - \cos^2(i)\}}}{v_s - \{R\Omega_e \cos(i)\}} , \qquad (B\text{-}8)$$

which is equation (4.56).

The spherical triangle Sine Rule, applied to triangle snm in the figure gives

$$\sin(Y_a) = \frac{\sin(L)}{\sin(i)} , \qquad (B\text{-}9)$$

where

$$Y_s = \Omega_s t . \qquad (B\text{-}10)$$

Therefore

$$\cos^2(L) = 1 - \{\sin^2(i)\sin^2(\Omega_s t)\} . \qquad (B\text{-}11)$$

Substitution into (B-8):

$$\tan(Y_a) = \frac{R\Omega_e \sin(i) \cos(\Omega_s t)}{v_s - \{R\Omega_e \cos(i)\}} = C \cos(\Omega_s t) , \qquad (B\text{-}12)$$

where C is a constant.

Equation (B-12) may now be differentiated with respect to time t by using

$$\frac{dY_a}{dt} = \frac{dY_a dx}{dx\, dt} . \qquad (B\text{-}13)$$

If the substitution,

$$x = \tan(Y_a) , \qquad (B\text{-}14)$$

is used, then

$$\frac{d}{dx}\left\{\frac{\arctan(x/a)}{a}\right\} = (a^2 + x^2)^{-1} , \qquad (B\text{-}15)$$

with

$$a = 1 . \qquad (B\text{-}16)$$

Therefore $$\frac{dY_a}{dx} = \frac{1}{1 + \{C^2 \cos^2(\Omega st)\}} . \qquad \text{(B-17)}$$

Differentiation of (B-14) gives

$$\frac{dx}{dt} = - C\Omega_s \sin(\Omega_s t) , \qquad \text{(B-18)}$$

and hence the result given in the text as equation (4.57):

$$\frac{dY_a}{dt} = - \frac{C\Omega_s \sin(\Omega_s t)}{1 + \{C^2 \cos^2(\Omega_s t)\}} , \qquad \text{(B-19)}$$

with

$$C = \frac{R\Omega_e \sin(i)}{v_s - \{R\Omega_e \cos(i)\}} . \qquad \text{(B-20)}$$

REFERENCES

No.	Author	Title, etc
1	R. Welch W. Marko	Cartographic potential of a spacecraft line-array camera system: Stereosat. *Photogrammetric Engineering and Remote Sensing*, **47**, 8, 1173-1185 (1981)
2	A.P. Colvocoresses	An automated mapping satellite system (Mapsat). *Photogrammetric Engineering and Remote Sensing*, **48**, 10, 1585-1591 (1982)
3	British Aerospace plc	*OMI - A Feasibility Study*. Technical Report, September 1987
4	S.A. Hempenius A.S. Marwaha A. Murialdo W. Ren-Xiang	Characteristics of the second generation Earth observation satellites. *ITC Journal*, 21-33 (1983)
5	V. Ashkenazi	Satellite positioning techniques. In: *Proceedings of a Remote Sensing Workshop*, Nottingham University, May 1984, edited by M.D. Steven, A.H. Dodson and P.M. Mather.
6	R. Welch	Measurements from linear array camera images. *Photogrammetric Engineering and Remote Sensing*, **46**, 3, 315-318 (1980)
7	R. Welch	Impact of geometry on height measurements from MLA digital image data. *Photogrammetric Engineering and Remote Sensing*, **49**, 10, 1437-1441, (1983)
8	J. P. Snyder	Geometry of a mapping satellite. *Photogrammetric Engineering and Remote Sensing*, **48**, 10, 1593-1602 (1982)
9	A. Moccia S. Vetrella	Different problems of space stereoscopic observation. In: *Proceedings of the EARSeL/ESA Symposium*, pp. 181-187, Strasbourg, 31 March-3 April 1985.

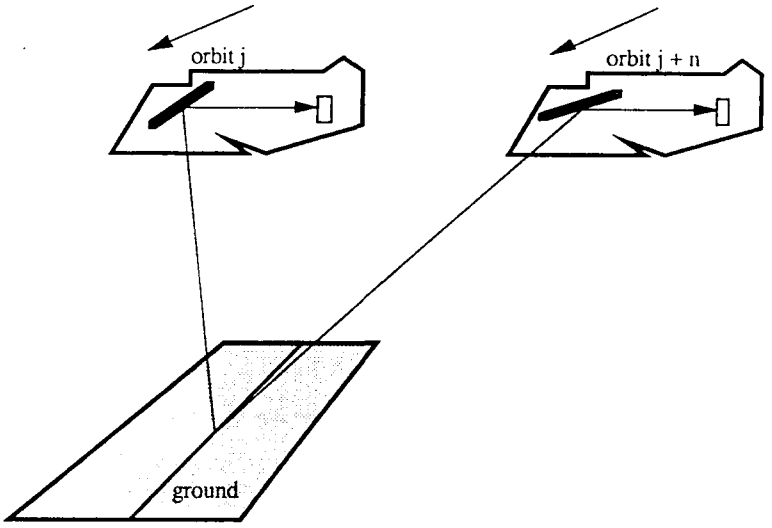

Fig 1 The generation of stereoscopic image pairs by SPOT-1

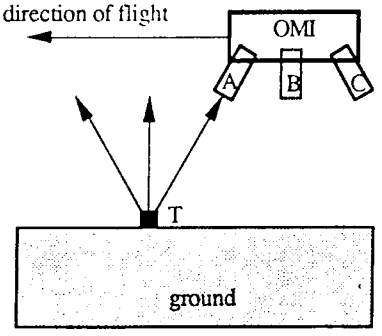

Fig 2 Telescope configuration for along-track stereoscopy

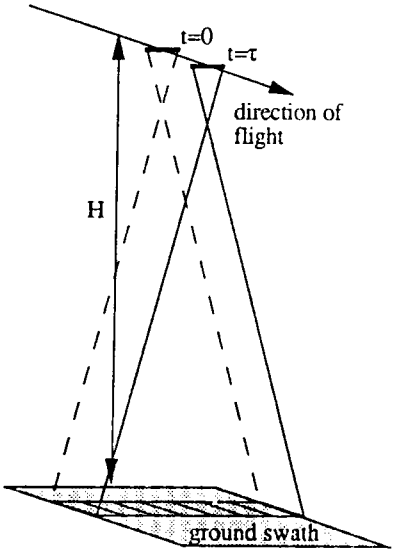

Fig 3 'Pushroom' imaging

Figs 4&5

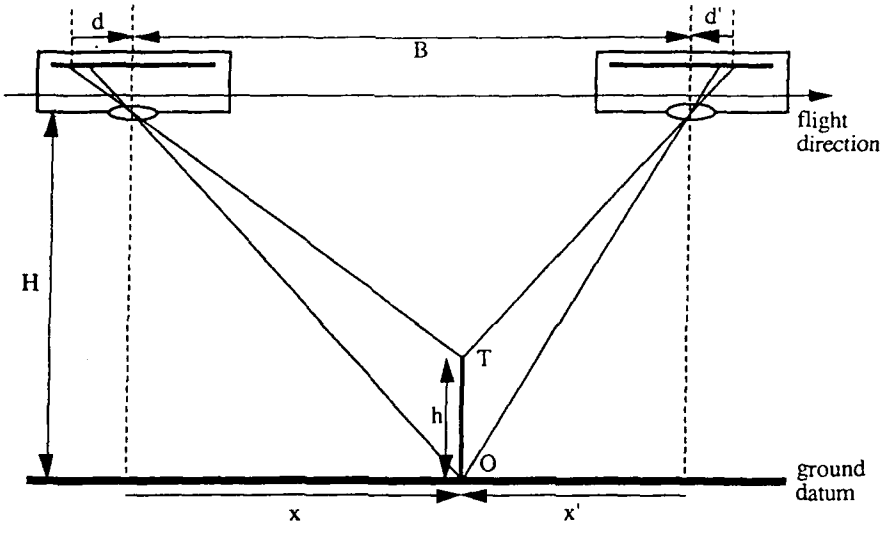

Fig 4 Along-track stereoscopy

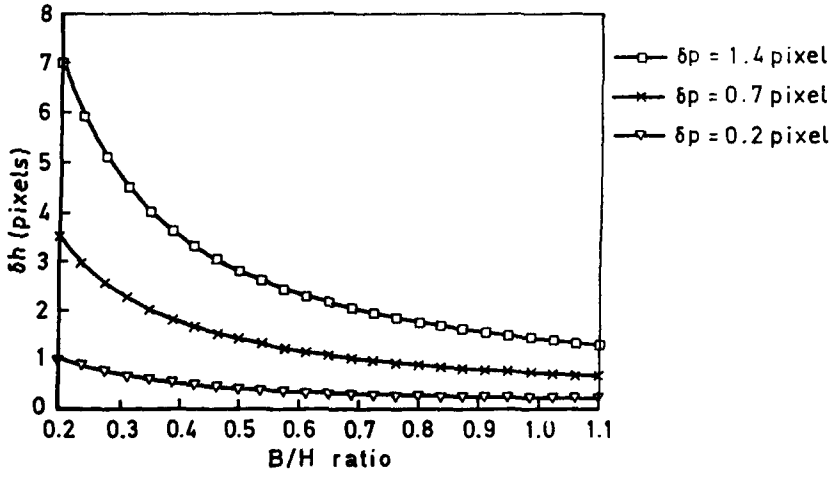

Fig 5 Height error δh as a function of B/H (assuming a flat Earth)

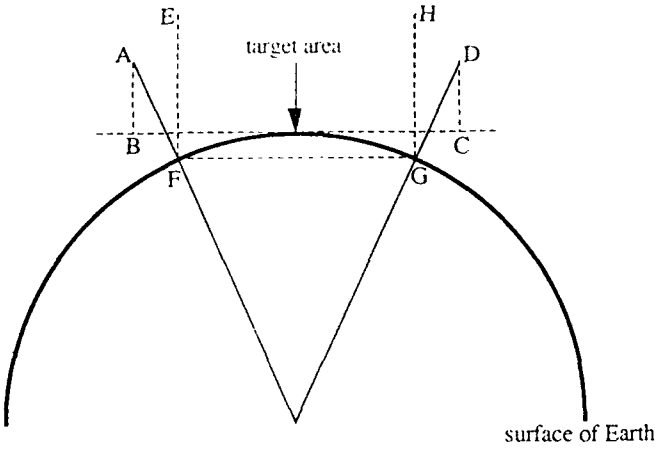

Fig 6 The effect of Earth curvature on B/H

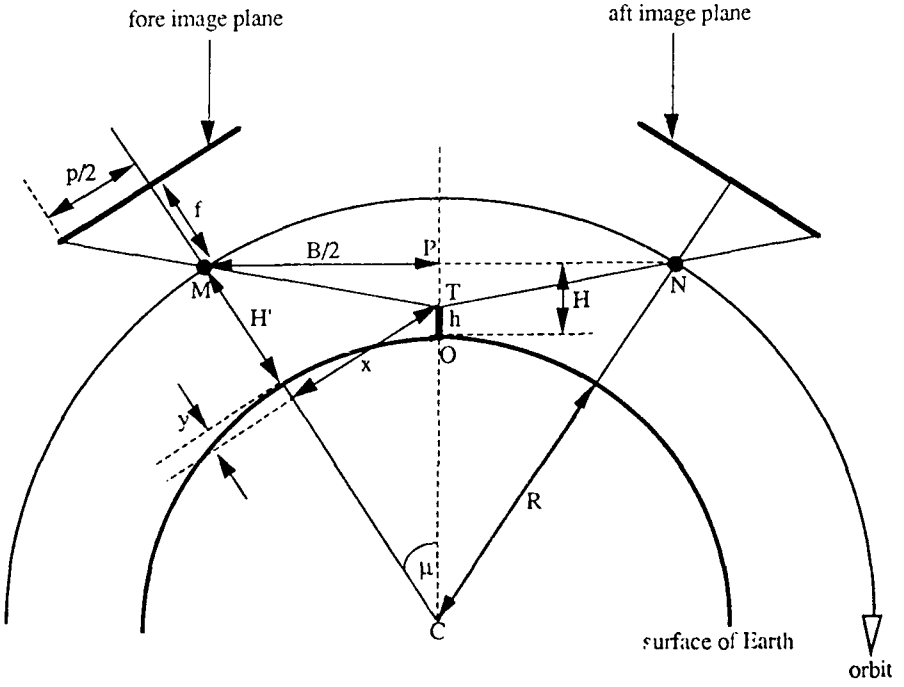

Fig 7 The effect of Earth curvature on along-track geometry

Figs 8&9

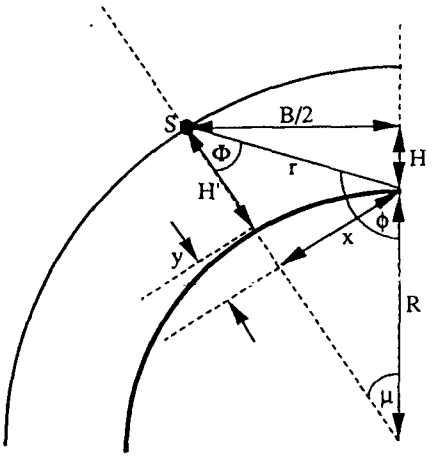

Fig 8a Along-track viewing

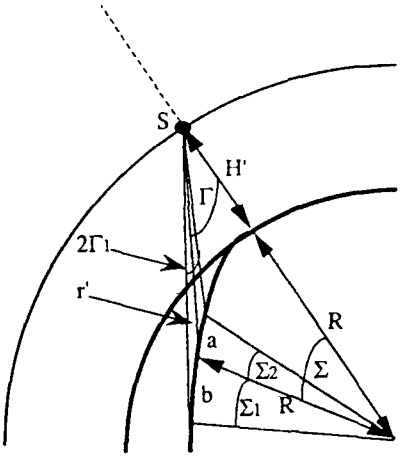

Fig 8b Cross-track viewing

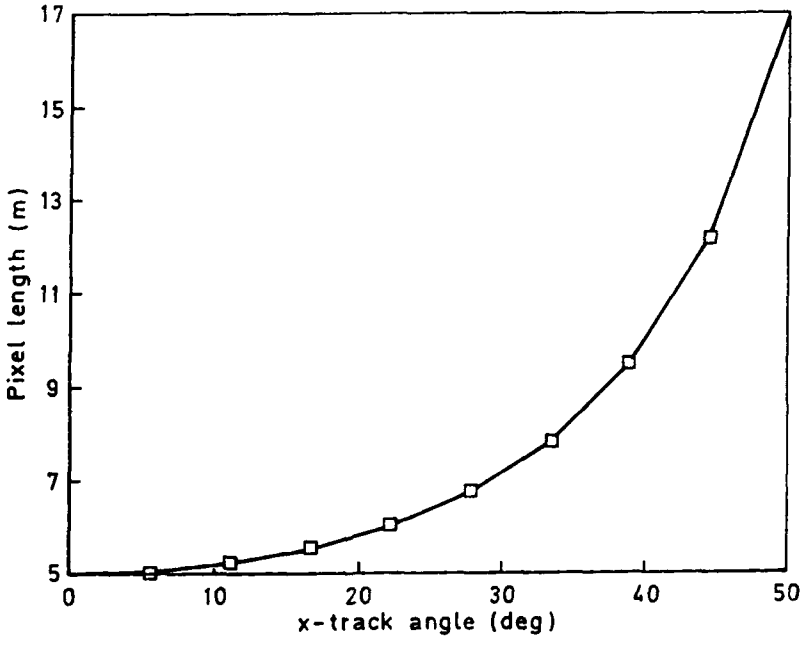

Fig 9 Variation of cross-track pixel length with cross-track angle

TR 90032

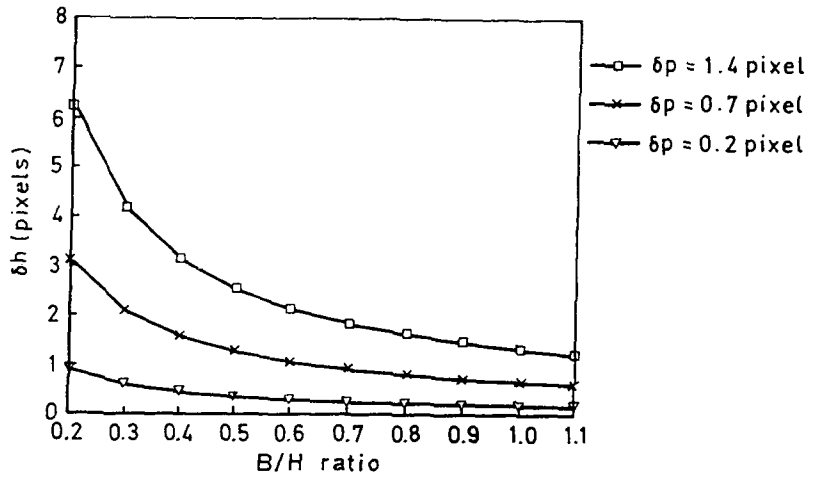

Fig 10 Height error δh as a function of B/H (assuming a spherical Earth)

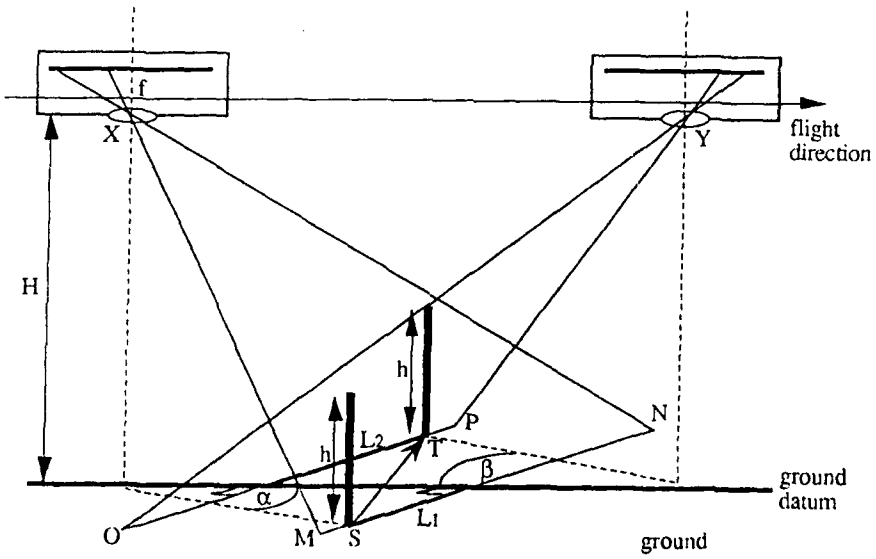

Fig 11 Stereo-geometry of a moving target

Figs 12&13

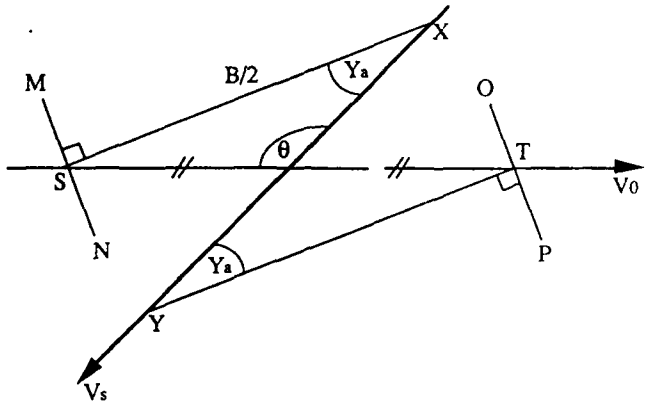

Fig 12 Geometry of yaw steering

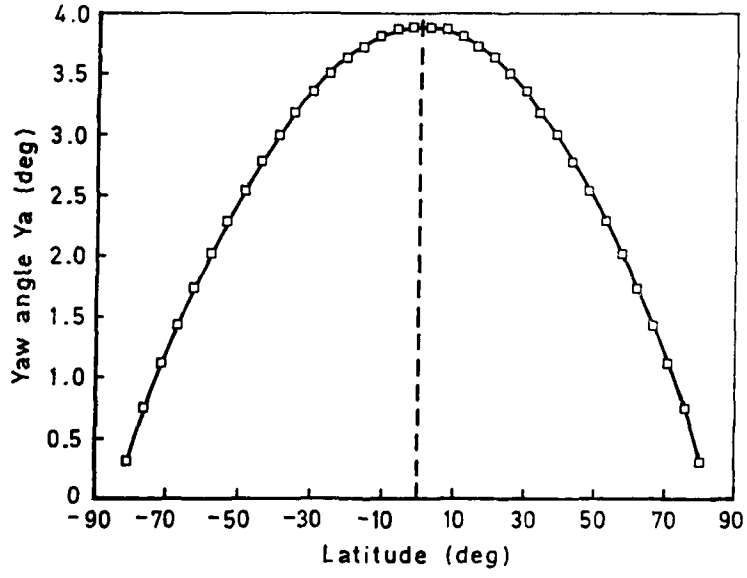

Fig 13 Variation of yaw angle with latitude

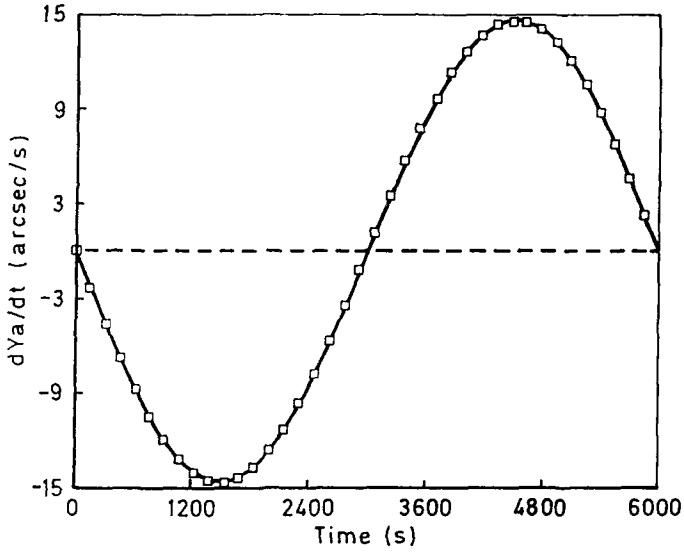

Fig 14 Variation of rate of change of yaw angle with time

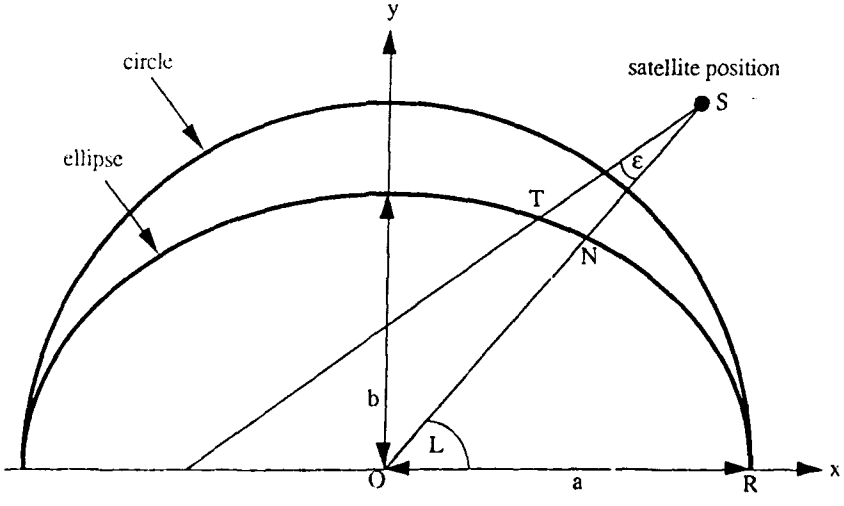

Fig 15 The effect of an oblate surface on image scale and area coverage

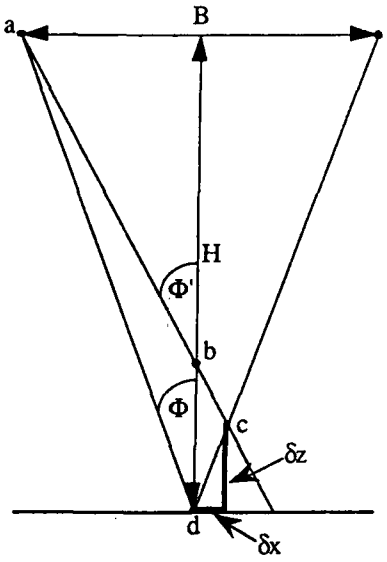

Fig 16 Geometry of a pointing error

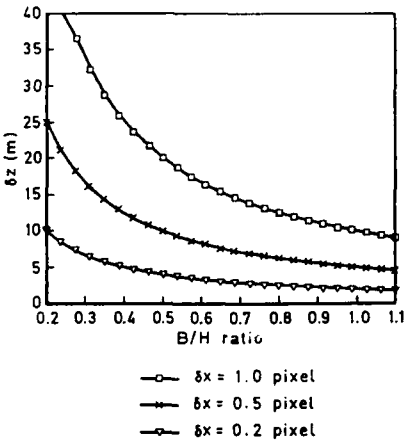

Fig 17 Spot-height error δz as a function of B/H

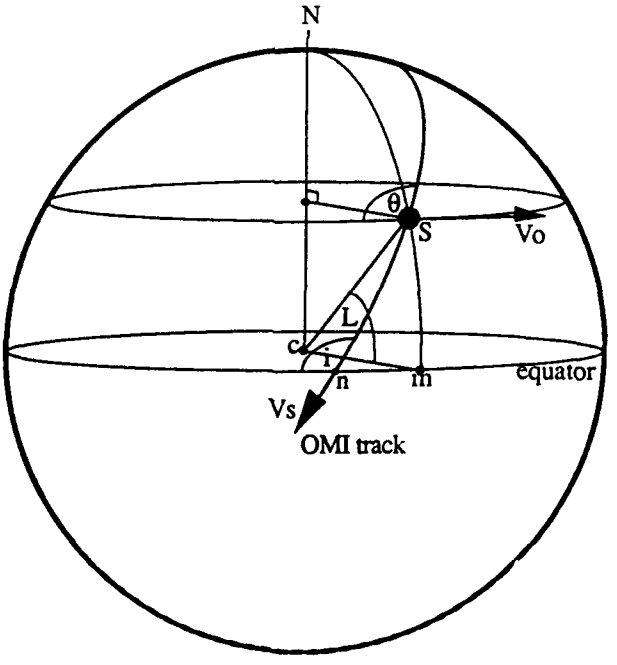

Fig 18 OMI track projected onto the Earth

REPORT DOCUMENTATION PAGE

Overall security classification of this page

UNLIMITED

As far as possible this page should contain only unclassified information. If it is necessary to enter classified information, the box above must be marked to indicate the classification, e.g. Restricted, Confidential or Secret.

1. DRIC Reference (to be added by DRIC)	2. Originator's Reference	3. Agency Reference	4. Report Security Classification/Marking
	RAE TR 90032		UNLIMITED

5. DRIC Code for Originator	6. Originator (Corporate Author) Name and Location
7673000W	Royal Aerospace Establishment, Farnborough, Hants, UK
5a. Sponsoring Agency's Code	6a. Sponsoring Agency (Contract Authority) Name and Location

7. Title: The stereoscopic geometry of the remote sensing 'Optical Mapping Instrument'

7a. (For Translations) Title in Foreign Language

7b. (For Conference Papers) Title, Place and Date of Conference

8. Author 1. Surname, Initials	9a. Author 2	9b. Authors 3, 4	10. Date	Pages	Refs.
Wells, N.S.			June 1990	41	9

11. Contract Number	12. Period	13. Project	14. Other Reference Nos.
			Space 678

15. Distribution statement

(a) Controlled by – Head of Space Department

(b) Special limitations (if any) –

If it is intended that a copy of this document shall be released overseas refer to RAE Leaflet No.3 to Supplement 6 of MOD Manual 4.

16. Descriptors (Keywords) (Descriptors marked * are selected from TEST)

17. Abstract

This Report examines the geometrical principles of stereoscopic remote sensing upon which the proposed Optical Mapping Instrument system is based. Consideration is given to the cartographic potential of the system in terms of constraints that arise from the viewing geometry, and conclusions are reached concerning the required accuracy and stability of the instrument.

F5910/1

DAL Form A143 (revised October 1990)